Int J Fract (2007) 148:281–290
DOI 10.1007/s10704-008-9201-y

ORIGINAL PAPER

Cycles of sub-critical tensile and shear alternating fracturing in diminishing dimensions, under tensile loading

Dov Bahat · Avinoam Rabinovich · Vladimir Frid · Franz J. Brosch

Received: 5 June 2007 / Accepted: 26 March 2008 / Published online: 18 April 2008

Abstract A microscopic study reveals that when the curvature of striae that mark the fracture surface of PMMA glass with a chevron pattern increase beyond the critical angle, $\mu c = 3° \pm 2°$, a breakdown into alternating tensile dark zones, and bright, ragged shear zones occurs. This breakdown was repeated in primary, secondary and tertiary cycles in diminishing scales. The secondary and tertiary breakdowns occurred exclusively in the shear zones. Similar breakdowns were found in chevron patterns on the fractured surface of a silicate glass ceramics. Due however to their different properties, certain differences were identified between the two materials in their breakdown characteristics, e. g. in the glass ceramic $\mu c = 20° \pm 2°$. A similar primary breakdown was also identified on tensile fractures cutting rocks in geological outcrops. In the glass ceramic the interface angle ϕ, which the striae form with the fracture boundary, decreased from $32° \pm 2°$in the early stage of the striae growth at relatively low velocity, to $13° \pm 2°$ during their advanced growth, at greater velocity, demonstrating that ϕ is a good tool for monitoring the change in fracture velocity in a given material. It was found that four interconnected factors determine the geometries and breakdown styles of the chevron pattern: (1) the curvatures of the fracture front and that of the striae which intersect each other orthogonally, (2) the influence of the fracture boundaries, (3) the material properties, such as stiffness, and (4) the fracture velocity in the material.

Keywords Fractography · Chevron · PMMA · Glass ceramic · Tensile and shear zones

D. Bahat (✉) · V. Frid
Department of Geological and Environmental Sciences, Ben Gurion University of the Negev, POB 653, Beer Sheva 84105, Israel
e-mail: Bahat@bgu.ac.il

D. Bahat · A. Rabinovich · V. Frid
The Deichmann Rock Mechanics Laboratory of the Negev, Negev, Israel

A. Rabinovich
Department of Physics, Ben Gurion University of the Negev, POB 653, Beer Sheva 84105, Israel

F. J. Brosch
Institute of Engineering Geology and Applied Mineralogy, Technical University Graz, Rechbauerstrasse 12, Graz 8010, Austria

1 Introduction

Chevron markings (also termed herringbone) mark the fractured surfaces of many metals and alloys (e. g. Hertzberg, 1975, p. 291; Hull 1999, p. 9) (Fig. 1a). They also occur in ceramics (Morrell 1995), silicate glasses (Orr 1972), polymer glasses and other technological materials (Fig. 1b). Plume markings approximate the chevron markings; they ubiquitously mark the surfaces of fractures in rocks (termed joints), which occur in geological outcrops (e. g. Syme Gash 1971; Hull 1999, p. 251) (Fig. 1c), where they sometimes reach tens of meters in length (Bahat 1991, p. 291).

Chevron markings consist of many striae (also termed lances), which initially propagate in straight lines and maintain parallelogram-shaped cross sections (Fig. 1d). However, as the striae curve to adjust to the curving fracture front, which they always intersect orthogonally, they display arrays of radial, curving ridges and valleys (characterized as tensile products) that form under fatigue conditions of sub-critical fracture velocities in chevron patterns (Hull 1999, pp. 245, 246) and in plumes (Bahat 1979). The present study concerns sub-critical, alternating tensile and shear components of striae, which form repeatedly in decreasing scale on the fracture surfaces of PMMA glass and silicate glass ceramics. A somewhat similar fracture pattern also occurs in plumes, collected from geological outcrops. Accordingly, the concept that brittle materials fail by shearing is addressed at the end of the discussion.

2 Fracture in the PMMA

We examined the microstructure of some uniquely well-displayed chevron markings which decorated the two fractured surfaces of two pieces of PMMA glass, retrieved from a broken motorcycle windscreen (Fig. 2a). The size of the two reconstructed pieces was 132 mm × approximately 23 mm × 4 mm. The fractured surfaces were inclined to the windscreen surfaces, forming an angle of about 45° with them. Penetration of the fracture surface marking was about 1 mm into the material. Fracture initiation clearly occurred in the circumference of the hole (h) through which a screw had fastened the windscreen to the motorcycle, providing the stress concentration needed to promote fracturing. Propagation of the fracture in the right piece was toward the right and the propagation of the fracture in the left piece was toward the left (lateral arrows). In the fracture on the left piece of PMMA glass the initial straight striae curve towards the fracture boundaries and assume the pattern of chevron markings.

An enlargement of a part of the left piece reveals intriguing micro-fracture features of the chevron markings (Fig. 2b). Striae that start propagating along straight trajectories split into dark, smooth tensile valleys (tv), which alternate with light, ragged shear elevated rims (sr) (Fig. 2c). The splitting starts at a critical median angle, $\mu c = 3° \pm 2°$. The individual smooth tensile zones are marked by delicate concentric rib marks, whose convex sides face the direction of fracture propagation (rm). Some of the alternating tensile valleys are wide, while others are narrow. The valley marked by (nv) is very narrow, creating an almost complete superposition of its two adjacent shear zones. The valleys are continuously elongated. In contrast, the individual ragged shear zones are further split into numerous secondary alternating tensile and shear fractures. These form parallel "slices" (s), which are oriented orthogonally to the boundaries between the primary tensile and shear zones. The interface angle ϕ, which the striae form with the fracture boundary varies from $66° \pm 2°$ to $70° \pm 2°$. The concentric rib marks representing the fracture front at various stages of the fracture propagation (Murgatroyd 1942), meet the striae orthogonally (Fig. 2b, c).

A magnification of a part of Fig. 2b discloses tertiary fracturing of the secondary shear zones (Fig. 2d), repeating the orthogonal relationship as described above. The thicknesses of the primary shear zones at the maxima of several striae are 0.5–0.8 mm (Fig. 2b, d), and the corresponding maxima of the secondary shear zones are in the 0.06–0.08 mm range (Fig. 2d). The secondary shear zones are sub-divided into some 8–12 tertiary pairs of tensile and shear zones (Fig. 2d). The thicknesses of these latter shear zones ranges between 0.009 mm and 0.011 mm. No further sub-division could be detected using the chosen optical system.

The fractured PMMA was examined by the polymeric polarizer Tech specTM linear polarizing laminated film, thickness-0.74 mm, manufactured by Edmund industrialoptics. Under polarized light the tensile zones remain dark, whereas many shear zones display a white color caused by double refraction. The double refraction is not evenly spread across the individual shear zones of the secondary fracturing (Fig. 2e). Several secondary shear zones display tertiary alternating dark and white colors (arrows in Fig. 2e).

Finally, the specimen under investigation (Fig. 2a) was retrieved from a broken motorcycle windscreen, so that the fracture conditions are not known, which is a drawback. Nevertheless, the exceptionally clear fracture surface features of this specimen, which disclose the multi-stage/multi-size fracture characteristics in such extreme detail, seem to justify our attention.

To the best of our knowledge no similar fracture features have been, either simulated or described before now.

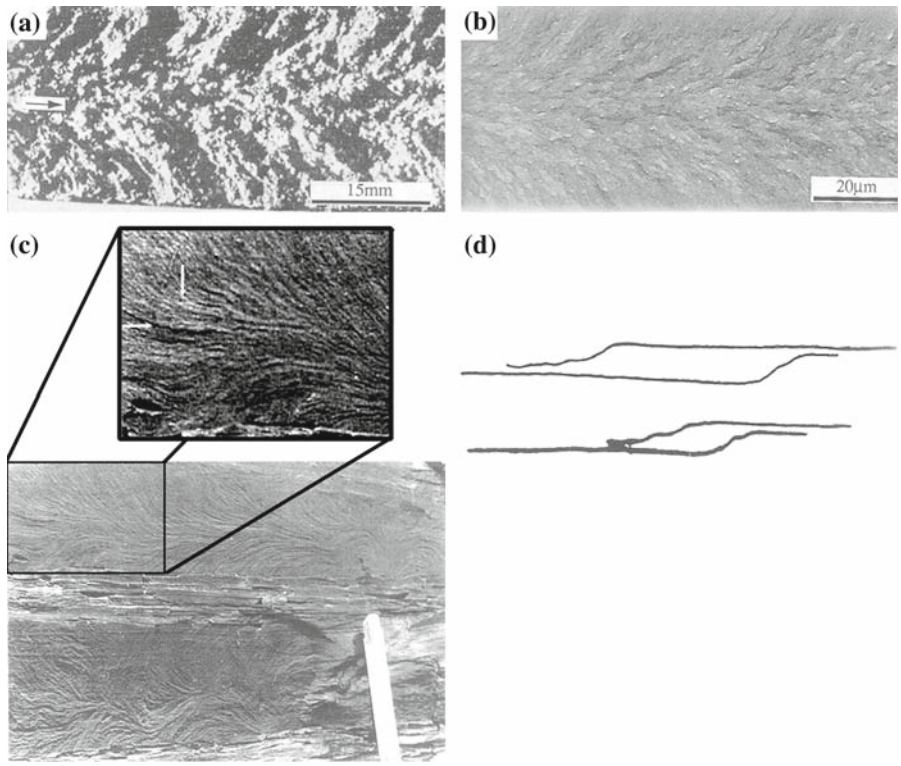

Fig. 1 (**a**) Chevron pattern in low-alloy steel (from Hull 1999, p. 9). (**b**) Chevron pattern in silica-based-sol–gel (from Hull 1999, p. 9). (**c**) Two plumes decorating joints that cut Devonian siltstone from the Appalachian Plateau, N.Y., propagating towards left. The ruler length is 20 cm. Frame of inset is marked (from Bahat and Engelder 1984). *Inset in c*. A magnified part of Fig. 1c, showing alternating radial zones of dark tensile valleys (horizontal arrow) and brighter shear ridges (vertical arrow), resulting from a primary breakdown. (**d**) Non-scaled, ross sections of two striae consisting of four planes, which approximate the parallelogram shape. Each parallelogram is made of two parallel straight surfaces (sub-horizontal), and two somewhat curved surfaces (modified after De Freminville 1914, also, Bahat 1991, p. 69)

3 Fracture in the glass ceramic

A silicate glass ceramic containing minute crystals (<1 mm), causing it to behave like glass, was fractured by uniaxial compression. Details of the material properties and experimental procedure are given in Bahat et al. (2002). Upon failure, the glass ceramic (size $104 \times 30 \times 20$ mm) fractured under tension along the specimen axis into two unequal parts, which were marked by chevron patterns. The fractured surface of the larger part is divided into three sectors: Sectors I and II formed in an early continuous fracturing process, while sector III formed later, discontinuously on a surface that cuts the surface which contains sectors I and II at an angle of 15° (Fig. 3a, b).

Sector I is marked by straight and slightly curved striae that penetrate some 5 mm into the material (Fig. 3a), maintaining the typical striae cross section (Fig. 1d). However, as the striae curve through $\mu c = 20° \pm 2°$, they break down into primary and secondary tensile and shear zones (sector II). The interface angle ϕ varies between $13° \pm 2°$ and $32° \pm 2°$ (Fig. 3a).

The secondary fracturing into alternating dark-smooth tensile zones and light-ragged shear zones is shown in Fig. 3b. The secondary pairs of tensile and shear zones are orthogonal to the boundaries of the primary fracturing (Fig. 3b). However, the tensile and shear zones that formed by the tertiary fracturing are not perpendicular to the boundaries of the secondary paired zones. Instead, they are oriented sub-parallel to it (Fig. 3c).

Another typical feature is the fracture irregularity: The tensile zones are considerably wider than the shear zones, and there are occasional repetitions of more

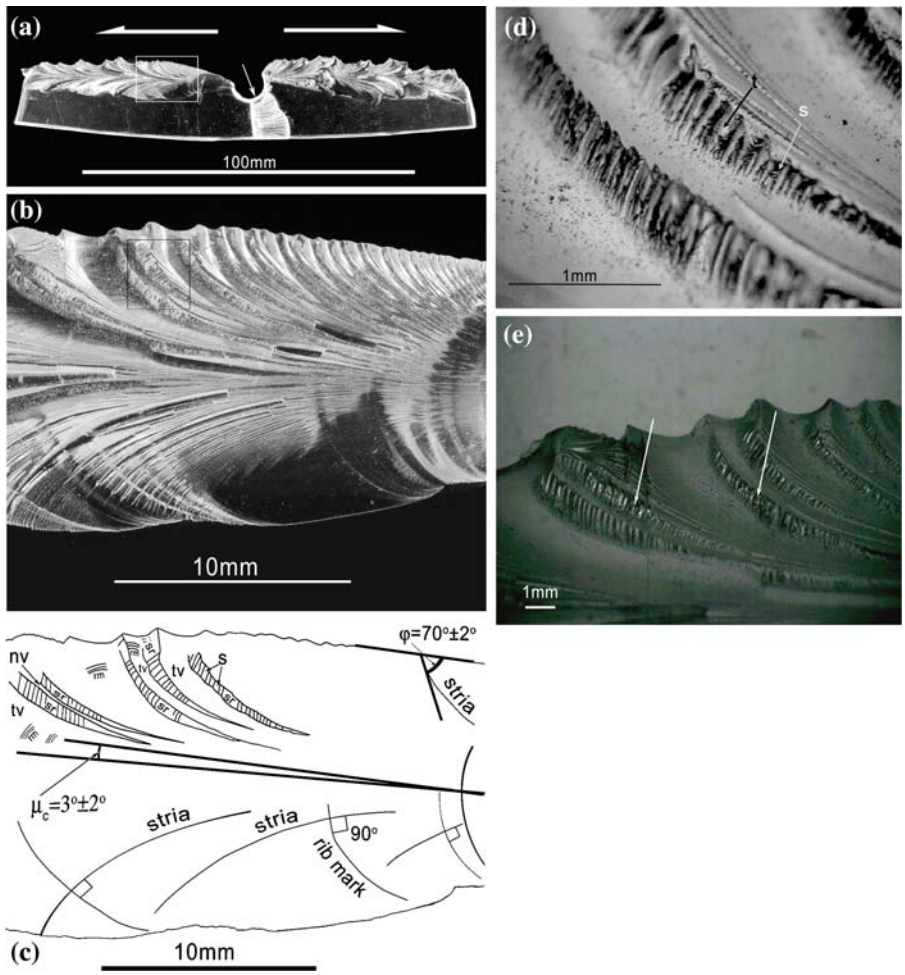

Fig. 2 (**a**) A general view of the two fractured pieces combined to the original long plate of a PMMA glass, showing the broken hole at center (inclined harrow). Two 'straight plumes' propagate to opposite directions (lateral arrows). The frame covers the approximate area shown in **b** and **c**. (**b**) is a magnified part of **a**, depicting the left fracture of the PMMA glass, which propagated from right to left, showing curving striae and concentric rib marks crossing each other orthogonally. The frame shows the area of **d**. (**c**) is a drawing of **b**, defining the various fractographic components. See text for the explanation of these features. (**d**) Magnified primary shear ridges. The ridge in the center of the picture (see frame in **b**) shows alternating shear (s) ragged surfaces and tensile (t) flat smooth surfaces that formed by a secondary breakdown. The secondary shear zones (parallel to the white arrow) are segmented by a tertiary fracturing into alternating tensile and shear zones, which are oriented sub-orthogonal to the white arrow. (**e**) The left upper part of **b** is photographed under polarized light. A white color caused by double refraction is selectively residing on the shear surfaces that formed by the secondary fracturing, bridging adjacent dark tensile surfaces. Several secondary shear zones (arrows) display vertical arrays of alternating dark and white colors of the tertiary zones

than one tensile zone between two neighboring shear zones (Fig. 3b). Also, the tensile and shear zones deviate from the rectangular shapes, and many of these zones end with tips with sharp edges. There are also light streaks within the tensile zones (possibly shear zones?) and unexplainable ''scars'' next to the shear zones in sector II (Fig. 3b). The thickness of the shear zones from the primary, secondary and tertiary scales vary considerably, with primary being between 0.1 mm and 0.8 mm, secondary being between 0.01 mm and 0.05 mm, and tertiary being between 0.005 mm and 0.025 mm.

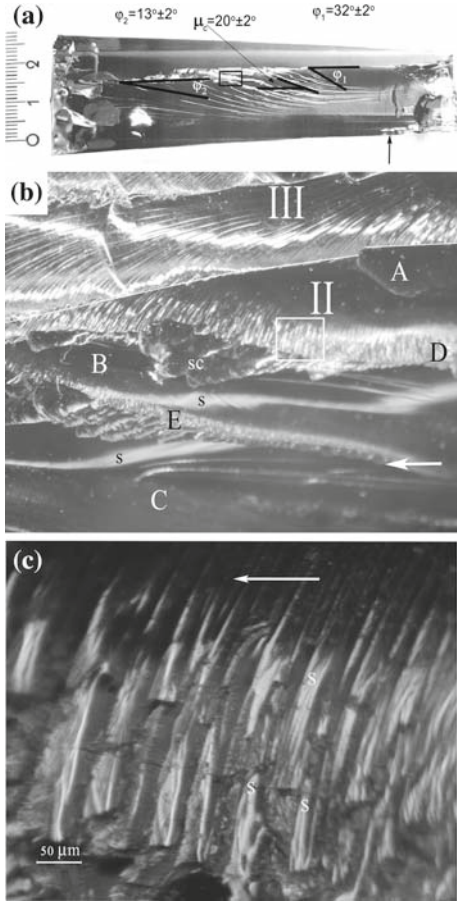

Fig. 3 (**a**) Striae on a fractured surface of a glass ceramic, initiate above the vertical arrow and propagate from right to left. They start propagating along straight trajectories and gradually curve towards the fracture boundaries, most of them above, and a few below the straight line (after Bahat et al. 2002). The square frames the area shown in **b**, $\mu c = 20° \pm 2°$, and ϕ varies between $\phi_1 = 32° \pm 2°$ and $\phi_2 = 13° \pm 2°$. Ruler in cm. (**b**) A magnified area framed in **a**, shows sector II below, separated by a solid white line from sector III above. Three tensile zones (A, B, C), are separated by two shear zones (D and E) in sector II. The shear zones are of unequal dimensions. The tensile dark zones are marked by occasional light streaks (s). Some additional "scars" (sc) are also identified in sector II. Fracture propagation from right to left. The frame defines the area shown by **c**. (**c**) A magnification of a primary shear zone (the frame in **b**), showing sub-vertical dark tensile valleys alternating light shear ridges that parallel each other. While the dark zones maintain approximately their same width, the light zones display many deviations from it, including, sub-parallel tertiary fracturing in the form of splits (s), and narrowing of the tertiary fractures at their (mostly upper) edges. Fracture propagation is from right to left

4 Fracture in rocks

Plumes markings decorate tensile fractures (joints) in many rocks, often showing arrays of curving radial ridges and valleys. A magnification of this fractography reveals primary fracturing, displaying alternating dark-smooth tensile zones and light-ragged shear zones (inset in Fig. 1c). This repeats the same pattern of primary fracturing that occurs in the chevron structures of the PMMA and glass ceramic. However, due to the graininess of the material, they do not disclose any structural details (Fig. 1c). Hence, the identification of secondary (and tertiary?) fracturing remains a matter for future research.

5 Discussion

5.1 Comparison of fracture properties in the PMMA and glass ceramic

There are similarities and differences in the fracture styles of the chevron patterns in the PMMA and the glass ceramic. The main similarity is the cycle of fracturing into alternating dark, smooth tensile zones, and bright, ragged shear zones in diminishing dimensions, particularly in the primary and secondary stages.

In detail however, there are differences in the fracture characteristics of the two materials:

1. The curving angles (Figs. 2c and 3a) at the point of breakdown of the striae into tensile and shear zone pairs are considerably different, $\mu c = 3° \pm 2°$ in the PMMA and $\mu c = 20° \pm 2°$ in the glass ceramic.
2. The interface angle which the striae form with the fracture boundary ϕ (Figs. 2c and 3a), is far smaller in the glass ceramic than in the PMMA glass: It ranges between $13° \pm 2°$ and $32° \pm 2°$ in the former, and between $66° \pm 2°$ and $70° \pm 2°$ in the latter.
3. In the PMMA there are regularly alternating tensile and shear zones of similar size and shape in the primary, secondary and tertiary stages. Particularly, the thicknesses of the secondary and tertiary shear zones are roughly uniform, displaying approximately rectangular shapes (Fig. 2b, d). On the other hand, in the glass ceramic there is less regularity. The tensile zones are considerably wider than the shear zones, and there are occasional repetitions of more than one tensile zone between

two neighboring shear zones. Also, the tensile and shear zones deviate from the rectangular shapes, and many of the tips of these zones end as sharp edges (Fig. 3b, c).

4. The orientation of the tertiary fracturing differs in the two examined materials: The tertiary zones are orthogonal to the direction of the secondary zones in the PMMA (Fig. 2d), but are parallel to the secondary zones in the glass ceramic (Fig. 3c).
5. Sector III exists in the glass ceramic (Fig. 3b) but not in the PMMA.

5.2 The breakdown mechanism of the chevron fracture pattern

Four interconnected factors determine the geometry and breakdown style of the chevron pattern: (1) the curvature of the fracture front and that of the striae that intersect it orthogonally, (2) the fracture boundaries, (3) properties of the material, such as stiffness, and (4) the fracture velocity of the material.

Straight striae form when a slight rotation of the tensile principal stress axis occurs in a plane perpendicular to the direction of fracture propagation, and this is associated with mixed modes I and III loading on the fracture surface (Sommer 1969; Bonamy and Ravi-Chandar 2005). This loading results in an instability that leads to a breakdown of the initial single fracture into striae made up of multiple fractures. Generally, the cross section of each stria is made up of four planes, which together approximate a parallelogram shape consisting of two parallel smooth, flat surfaces, at broad angles to two somewhat warped surfaces (Fig. 1d).

However, when the striae curve a more complex breakdown occurs, as is shown by the chevron pattern. The chevron pattern is generally long and narrow (Figs. 1a, 1b, 2a and 3a). Analogically, plume markings cut only thin rock layers (Roberts 1961). In such cases, the fracture boundaries (of small specimens in the laboratory and larger rock layers in the field) have a great deal of influence on the process, primarily by retarding the fracture velocities (Tipper 1957). An increase in the striae curving is associated with a commensurate increase in the mode III/mode I ratio, which is accompanied by the creation of the alternating smooth, flat tensile zones and the warped, ragged shear zones. This is perfectly displayed by the fractured PMMA (Fig. 2a–e). The same applies to the fractured glass ceramic and rocks (Figs. 3a and 1c) although it is less apparent due to the inertia of faster propagation in the glass ceramic (see below) and the graininess in the rock. Hence, straight striae that form normal to the fracture front at the center (farthest away from the fracture boundaries) must gradually increase their curvature as they come nearer the boundaries, where the zone differentiation is increased. To compensate, the retardation along the fracture boundaries results in maximum curvature of the fracture front at the center, with its convex side facing the direction of fracture propagation. The various rib marks that decorate the smooth, flat zones on the fractured PMMA (Fig. 2b, 2c) mark different propagation stages of the curved fracture front.

The morphological and double refraction differentiation between the smooth, flat tensile zones and the warped shear zones imply that while the newly formed tensile zones are stable, the shear zones remain unstable: The breakdown into many cracks and the double refraction occur only in the shear zones. Instability under dynamic conditions (i.e. above K_{Ic} fracture) appears to be similar in PMMA and glass (Sharon and Fineberg 1999). The present microscopic study reveals that basically, the same breakdown style occurs in different materials (PMMA, glass ceramic and rocks) under sub-critical conditions, though with some differences, as detailed above.

The curving angles at the breakdown of the striae into pairs of smooth, flat zones and warped zones are far smaller in the PMMA compared with that in the glass ceramic ($\mu c \sim 3^\circ$ and $\mu c \sim 20^\circ$, respectively). This indicates that in the less stiff material, PMMA, the breakdown is quicker than in the stiffer glass ceramic, and this material yields to the increase of the mode III/mode I ratio as the striae start to curve. Curving of the striae is considerably more advanced in the glass ceramic before the breakdown occurs.

The fracture velocities of the three examined materials were sub-critical. No actual information on the fracture velocity associated with the formation of the fractography of the PMMA (Fig. 2a) is known, but it was probably sub-critical, for the following reasons: (1) All the chevron markings are confined to the mirror plane, without traces of the mirror boundary, hackles or bifurcation which signify dynamic conditions. (2) The interface angle ϕ is around 70° in the fractured PMMA (Fig. 2c), due to slow propagation. The inertia of fast propagation would not allow such strong

rotation towards the free surface, and would result in smaller ϕ values (see for comparison the size of ϕ in the glass ceramic, below). (3) The double refraction in the PMMA indicates residual stresses in the material. High energy, post-critical fracturing would probably release all residual stresses.

The plume decorating the fracture in the rock (Fig. 1c) was also a product of sub-critical tension (Savalli and Engelder 2005).

The critical velocities (vc) below which sub-critical fractures occur, in PMMA and glass are approximately 400 m/s and 1500 m/s, respectively (Sharon and Fineberg 1999). The fracture velocity in the glass ceramic was $v \approx 1000$ m/s (Bahat et al. 2002), which is well within the sub-critical regime. In the glass ceramic the interface angle ϕ decreased from $32° \pm 2°$ in the early stage of the striae growth (while they were short) to $13° \pm 2°$ at their final stage of growth (Fig. 3a). This supports the idea that K_I and K_{III} increase with the rise of the fracture length, and therefore that the fracture velocity, v, increases as well, according to the well known equation $v = AK^n$, where A and n are constants. Accordingly, the increase in ϕ implies that the crack velocity increases throughout the early and final stages. Hence, inspecting ϕ along curving striae is a good tool for monitoring the change in fracture velocity in a given material.

Quite possibly, the slow, sub-critical fracture in the PMMA had sufficient time to execute repeated, systematic breakdowns in the material. It seems, on the other hand, that the inertia of the faster fracturing in the glass ceramic (though still being sub-critical), introduced deviations from the "well organized" systematic breakdown.

Thus, the cyclic effect of sub-critical, alternating, smooth, flat tensile zones and warped shear zones in diminishing dimensions increases with: The mode III/mode I ratio, the aspect ratio (length/width) of the fracture surface, and the interface angle, ϕ. This effect also increases with the decrease in: Fracture velocity, the material stiffness, and the critical curving angles at breakdown, μc.

5.3 On the concept that brittle materials fail by shearing

The present results, showing that curved striae in fractured materials contain both smooth, flat zones and warped, ragged zones, coincide with earlier observations by De Freminville 1914 and Preston 1931 (see elaboration in Bahat 1991, p. 68), which showed that striae walls consist of both flat and warped planes at broad angles to each other (Fig. 1d). Dark, flat tensile planes that alternate with bright, warped shear surfaces at high angles are also seen on large-scale tensile fractures (joints) in geological exposures (Fig. 4a).

Experiments using compression uniaxial and triaxial tests on chalk cylinders also show the two crack types (Bahat et al. 2001). These results show contrasting properties between surfaces that are formed by local tension and those that are formed by local shear stresses. While the former display smooth, gray, flat surfaces, the latter are white and ragged. Also, the tensile surfaces are oriented parallel or sub-parallel to the direction of compression, whereas the shear surfaces deviate from this orientation (Fig. 4b). It was found that the transitional angle between the two was $8° \pm 2°$.

Further support for the observations of alternating tensile and shear zones comes from investigations on en echelon cracks. These cracks are formed by mixed mode I and III. The en echelon cracks often occur in continuation of striae, suggesting similar fracture mechanisms. However, the alternating tensile and shear zones are generally larger in the en echelon cracks that reside in the fringe beyond the mirror boundary, than in the striae that occur within the mirror plane. The large size of these zones provides a clear view of the distinction between the tensile and shear zones (Fig. 4c). Analyses by Pollard et al. (1982) and Nicholson and Ejiofor (1987) as well as experimental results by Cooke and Pollard (1996) expand on the tensile vs shear mode products in en echelon cracks.

It has been seen that the increase in striae curving is associated with an increase in the mode III/mode I ratio. Consequently, the shear stress becomes relatively more pronounced than the tensile one. This change becomes apparent morphologically: While the dark, flat component of the striae is formed by local tension, the white, ragged step is created by local shear (Fig. 2b). These conditions are caused by the fracture boundaries, which effect the fracture process. The implication is that when remote tension is applied to a specimen with infinite dimensions only tensile failure occurs. On the other hand, sub-critical fracture propagation close to boundaries would lead to resolving the remote stress into local tensile and shear stress components, and that would

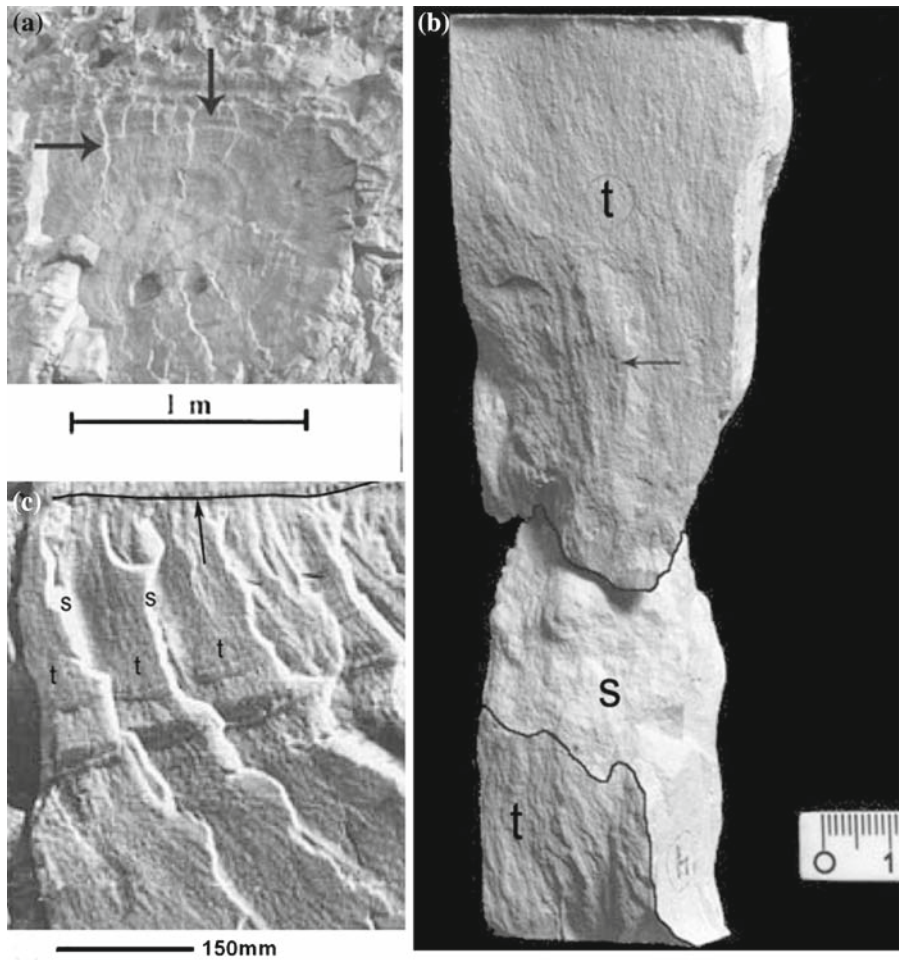

Fig. 4 (**a**) A mirror plane on a dark tensile fracture (joint) in a limestone outcrop, showing concentric rib marks (vertical arrow) and radial, bright striae (horizontal arrow) (the larger cavities show fracture nucleation sites). Scale is 1 m. (modified from Weinberger 2001). (**b**) Fractured chalk under uniaxial compression in the vertical axis direction. Two axial flat dark tensile fractures (t), which are relatively smooth, are displaced in order to show the inclined shear ragged, white fracture surface (s) (between upper and lower boundaries) (horizontal arrow shows the nucleation of a new parallel tensile fracture superposed on the older one). Scale is cm (from Bahat et al. 2001). (**c**) The lower part of a mirror plane of a joint at the upper part of the photograph, is separated by a mirror boundary (shown by an arrow) from the en echelon fringe below. The fringe consists of alternating flat dark tensile cracks (t) and ragged shear bright steps (s) (also termed bridges) (modified from Bahat et al. 2005, p. 135)

induce adjacent tensile and shear fractures (Figs. 2b and 4b).

5.4 Open question

In the PMMA the secondary pairs of tensile and shear zones are orthogonal to the boundaries of the primary fracturing (Fig. 2c), and the tertiary pairs of tensile and shear zones are orthogonal to the boundaries of the secondary fracturing (Fig. 2d). In the glass ceramic, on the other hand, the secondary pairs of tensile and shear zones are orthogonal to the boundaries of the primary fracturing (Fig. 3b), but the tertiary pairs of tensile and shear zones are sub-parallel to the boundaries of the secondary fracturing (Fig. 3c). It is unclear why the faster fracturing in the glass ceramic does not allow the tertiary pattern seen in the PMMA. This requires further attention.

6 Conclusions

The chevron pattern that has until now been considered to be a tensile sub-critical fracture surface morphology is proven to be a complex micro-structure of tensile and shear zones in both PMMA glass and in silicate glass ceramic.

Tensile loading in these materials results in curving striae that break down into alternating smooth, dark tensile zones, and bright, ragged shear zones. This breakdown occurs in three stages of diminishing dimensions: Primary, secondary and tertiary.

While the primary breakdowns take place on a flat tensile surface, the subsequent two types of breakdowns occur exclusively in the shear zones.

A comparison of the fracture behavior of PMMA and glass ceramic shows that there are similarities and differences in their systematic breakdown styles. The main similarity is in the cyclicity of fracturing, particularly in the primary and secondary stages. The differences are also significant.

Plumes that decorate the tensile fractures (joints) in many rocks often show arrays of curving radial ridges and valleys. A magnification of this fractography reveals primary fracturing, which displays alternating smooth, dark tensile zones and bright, ragged shear zones, repeating the same pattern of primary fracturing that occurs in the chevron structures of the PMMA and glass ceramic. However, due to the graininess of the material, they do not show any further fracturing.

In the PMMA the thickness of the primary, secondary and tertiary shear zones at their maxima are 0.5 mm to 0.8 mm, 0.06 mm to 0.08 mm, and 0.009 mm to 0.011 mm, respectively.

In the glass ceramic the thickness of the primary, secondary and tertiary shear zones at their maxima are 0.1 mm to 0.8 mm, 0.01 mm to 0.05 mm, and 0.005 mm to 0.025 mm, respectively.

Four interconnected factors determine the geometries and breakdown styles of the chevron pattern: (1) the curvature of the fracture front and that of the striae that intersect it orthogonally, (2) the fracture boundaries, (3) the material properties, such as stiffness, and (4) the fracture velocity of the material.

Generally, a cross section of each stria is made up of four planes, including two straight, parallel surfaces (tensile fractures) at broad angles to two somewhat curved surfaces (shear fractures).

However, when the striae curve the chevron pattern forms, in such a way that the fracture boundaries retard fracture velocities along them, resulting in the differentiating between shear and tensile zones, and compensating by maximum curvature of the fracture front at the center. All these things are associated with an increase in the mode III/mode I ratio as the curvature increases.

The morphological and double refraction differentiation between the tensile and shear zones imply that while the newly formed tensile regions are stable, the shear zones remain unstable.

The curving angles at the breakdown of the striae into tensile and shear zone pairs in PMMA are far smaller than those in the glass ceramic, indicating that in the less stiff material, PMMA, the breakdown is faster than in the stiffer glass ceramic.

It is demonstrated that the interface angle ϕ is a good tool for monitoring changes in fracture velocity.

Quite possibly, the slow, sub-critical fracturing in the PMMA had sufficient time to undergo repeated, systematic breakdowns. While on the other hand, the inertia of the faster (though still sub-critical) fracturing in the glass ceramic introduced deviations from the systematic breakdown.

Thus, the cyclic alternation of sub-critical tensile and shear fractures in diminishing dimensions increases with: The mode III/mode I ratio, the interface angle, ϕ. This effect also increases with a decrease in: The Fracture velocity, the material stiffness, and the critical curving angles at breakdown, μc.

Acknowledgements Eli Shimshilashvili most kindly took the micro-photos of the fractured PMMA. Or Bialik provided technical help.

References

Bahat D (1979) Theoretical considerations on mechanical parameters of joint surfaces based on studies on ceramics. Geol Mag 116:81–92

Bahat D, Engelder T (1984) Surface morphology on cross fold joints of the Appalachian Plateau, New York and Pennsylvania. Tectonophysics 104:299–313

Bahat D (1991) Tectonofractography. Springer-Verlag, Heidelberg

Bahat D, Rabinovitch A, Frid V (2001) Fracture characterization of chalk in uniaxial and triaxial tests by rock mechanics, fractographic and electromagnetic radiation methods. J Struct Geol 23:1531–1547

Bahat D, Frid V, Rabinovitch A, Palchik V (2002) Exploration via electromagnetic radiation and fractographic methods of fracture properties induced by compression in glass-ceramic. Int J Fracture 116:179–194

Bonamy D, Ravi-Chandar K (2005) Dynamic crack response to a localized shear pulse perturbation in brittle amorphous materials: on crack surface roughening. Int J Fracture 134:1–22

Cooke ML, Pollard DD (1996) Fracture propagation paths under mixed mode loading within rectangular blocks of polymethyl metha-crylate. J Geophys Res 101:3387–3400

De Freminville MCh (1914) Recherches sur la fragilité–l'éclatement. Rev Metall-Paris 11:971–1056

Hertzberg RW (1975) Deformation and fracture mechanics of engineering materials. Wiley, New York 605 pp

Hull D (1999) Fractography: observing, measuring, and interpreting fracture surface topology. Cambridge University Press, Cambridge

Morrell R (1995) Standardized guidelines for fractography of advanced ceramics-a view from Europe. Fractography of glasses and ceramicsIII Varner JR Frechette, VD Quinn, GD Ceramic Transactions 64:71–89. The American Ceramic Society.

Murgatroyd JB (1942) The significance of surface marks on fractured glass. J Soc Glass Technol 26:155–171

Nicholson R, Ejiofor IB (1987) The three dimensional morphology of echelon and sigmoidal mineral-filled fractures: data from North Cornwall.. J Geol Soc Lond 144:79–83

Orr L (1972) Practical analysis of fractures in glass windows, ASTM, Philadelphia, pp 21–23, 47.

Pollard DD, Segall P, Delaney PT (1982) Formation and interpretation of dilatant echelon cracks. Geol Soc Am Bull 93:1291–1303

Preston FW (1931) The propagation of fissures in glass and other bodies with special reference to the split-wave front. J Am Ceram Soc 14:419–427

Roberts JC (1961) Feather-fracture and the mechanics of rock jointing. Am J Sci 259:481–492

Savalli L, Engelder T (2005) Mechanism controlling rupture shape during subcritical growth of joints in layered rocks. Bull Am Geol Soc Am 117:436–449

Sharon E, Fineberg J (1999) Confirming the continuum theory of dynamic brittle fracture for fast cracks. Nature 397:333–335

Sommer E (1969) Formation of fracture "lances" in glass. Eng Fract Mech 1:539–546

Syme Gash PJ (1971) Surface features relating to brittle fracture. Tectonophysics 12:349–391

Tipper CF (1957) The study of fracture surface markings. J Iron St Inst 185:4–9

Weinberger R (2001) Joint nucleations in layered rocks with non-uniform distribution of cavities. J Struct Geol 23:1241–1254